lubricants

MDPI

Article

Research on Leakage Prediction Calculation Method for Dynamic Seal Ring in Underground Equipment

Xiaohui Xu [1,2], Xin Li [1,2,*], Fengtao Wang [1,2] and Chunmiao Xia [3]

[1] School of Mechanical Engineering, Anhui Polytechnic University, Wuhu 241000, China; xxh2021219@126.com (X.X.); wangfengt1985@163.com (F.W.)
[2] The Center of Mechanical Dynamics and Control Technology, Anhui Polytechnic University, Wuhu 241000, China
[3] School of Chemical and Environmental Engineering, Anhui Polytechnic University, Wuhu 241000, China; xiachunmiao@ahpu.edu.cn
* Correspondence: lx600526@126.com

Abstract: The leakage prediction calculation method for dynamic seal rings in underground equipment is presented in this paper. The framework of the method is given. The leakage prediction model is built. The non-Newtonian fluid interface element is brought in. The leakage prediction calculation method was developed based on the thermal–structural coupled method and the fluid–structural coupled method. A test is performed to validate the proposed method. It is proved that the film thickness of an O-ring made of nitrile rubber in pulling-in travel is thicker than that in pushing-out travel. The leakage of an O-ring made of fluororubber is larger than that of an O-ring made of nitrile rubber in the same environmental condition. The presented method is useful for predicting the sealing ability of dynamic seal rings in underground equipment. Evaluation costs will be reduced with the given leakage prediction calculation method.

Keywords: underground equipment; dynamic seal ring; leakage prediction; calculation method; finite element (FE)

Citation: Xu, X.; Li, X.; Wang, F.; Xia, C. Research on Leakage Prediction Calculation Method for Dynamic Seal Ring in Underground Equipment. *Lubricants* **2023**, *11*, 181. https://doi.org/10.3390/lubricants11040181

Received: 25 February 2023
Revised: 12 April 2023
Accepted: 17 April 2023
Published: 18 April 2023

1. Introduction

Nowadays, global oil resources are becoming depleted [1]. Deep wells are explored to obtain more oil resources [2–4]. Many kinds of underground equipment are developed [5]. As everyone knows, the underground environment is harsher than that on the ground. Underground equipment must endure a harsh environment, such as high temperatures and high pressure [6–8]. So, requirements for the reliability of underground equipment are stricter than that of common equipment on the ground. In this harsh environment, both rock mechanics and reliability need to be studied intensively [9].

A visualization technique that was used to investigate rock mechanics in an underground environment was developed by Xie et al. [10]. The mechanical behavior of rock under high-temperature conditions was studied by Yin et al. [11,12]. Both the uniaxial compression and the shear failure behavior were focused on. Gao et al. [13] researched the coal and rock in deep wells through an in situ mechanical experiment. They found that the mechanical strength of deep rock under engineering disturbances was smaller than conventional tri-axial strength. Mechanical properties and rock fracture theories were investigated by Feng et al. [14]. Basic theories for evaluating the stability of the reservoir and surrounding rock were presented. To solve the problem that the current sampling equipment owned insufficient holding pressure capability, an in situ condition-preserved coring (ICP-coring) system was developed by He et al. [15]. A pressure-holding controller was designed according to the Moho square cover principle. However, dynamic seal rings play an important role in underground equipment [16]. As influenced by high temperatures and high pressure in underground environments (the temperature generally reaches over fifty centigrade while pressure generally ranges from ten more MPa to dozens of MPa), dynamic seal rings in underground equipment are affected

by both the thermal domain and structural domain. If the seal ring cannot seal well, fluid distributing on both sides of the seal ring will be exchanged excessively, causing leakage. For underground equipment, not only stability but also accuracy for measurements will be significantly influenced by leakage.

The sealing behavior of seal rings in different kinds of equipment has been researched by many scholars. A three-dimensional simulation model was proposed by Zhu et al. to analyze the performance of a combined seal ring [17]. They found that the contacting pressure of the combined seal ring was significantly influenced by the thickness of the slip ring, the pressure of the working fluid medium and the compression amount of the O-ring. The influence of the pre-compression ratio of the O-ring, the material hardness of the O-ring and the thickness of the slip ring on the sealing performance was researched by Guo et al. via the FE software ANSYS Workbench [18]. The sealing performance of combined seal rings with different surface structures under maximum environment pressure, 20 MPa, was studied by Zhao et al. [19]. The influence of working pressure and pre-compression of the seal ring on the sealing performance was analyzed by Salant et al. by establishing a calculation model of the reciprocating hydraulic piston sealing device [20]. The relationship between sealing pressure and leakage amount was studied by Nikas et al. [21]. A numerical model for reciprocating rod matching with a rectangular seal ring was built. The influence of the structural parameters of the seal ring on the sealing performance was simulated by Chen et al. via ABAQUS software [22]. The distribution of temperature and stress of the non-contact seal was analyzed by Blasiak et al. [23]. Moreover, the effect of different structures on the sealing performance was also discussed. Mo et al. analyzed the sealing performance of the reciprocating seal ring used in petroleum devices [24]. They found that the maximum contacting pressure varied nonlinearly with the increment of sliding speed of the piston rod. Sukumar et al. investigated the sealing performance of seal rings via the FE method [25]. The sealing ability was improved by setting reasonable material parameters and process parameters. Chen et al. studied the influence of structural parameters of spiral grooves on the sealing performance based on the cavitation model [26]. The optimal range for each parameter was also proposed. A testing protocol was developed by Ahmed [27] to investigate the performance of common elastomeric seal rings, which were used in a liner seal assembly hanger. Ethylene propylene diene monomer (EPDM) and nitrile butadiene rubber (NBR) were selected as the materials of seal rings for the tests. The results revealed that elastomers' energization played a critical role in maintaining their sealing integrity.

These research studies have paid sufficient attention to the sealing performance of seal rings. However, many of them are focused on the seal ring in common equipment. Few studies have focused on the seal ring in underground equipment. Since the dynamic seal rings in underground equipment undergo harsh environments with high temperatures and high pressure, it is not convenient to predict the sealing ability of the seal rings via experimental ways. When designing a test rig, designers need to consider whether the devices are suitable for the test environment, and safety also needs to be taken into consideration. So, it is a time-consuming and money-consuming project to build a test rig that is used to simulate an underground environment.

As computer techniques developed, it became possible to predict the leakage of dynamic seal rings in underground equipment through numerical ways. However, it can be known from the literature that the presented numerical methods have not been applied to dynamic seal rings in underground equipment. Therefore, the leakage prediction calculation method for dynamic seal rings in underground equipment will be presented in this paper. A general framework of the leakage prediction calculation method will be given. Then, a leakage prediction model will be built, and non-Newtonian fluid interface elements will be brought in. The leakage prediction calculation method will be given at the end. The leakage amount of dynamic seal rings made of different materials under different environmental conditions will be measured through experimentation. The test results will be compared with the prediction results to validate the presented method. With the help of the method presented in this work, designers and engineers can predict the sealing

performance of dynamic seals in underground equipment through computer simulations instead of physical tests, which cost too much money and time.

2. Leakage Prediction Calculation Method for Dynamic Seal Ring in Underground Equipment

When the piston rod reciprocates linearly, the relative motion will give rise to the hydrodynamic effect in the sealing clearance. Contacting pressure between the seal ring and chamber will be held by the film. The surface of the seal ring will be separated by the film from the surface of the chamber. This kind of seal ring is called a dynamic seal ring. The system of the dynamic seal ring is shown in Figure 1.

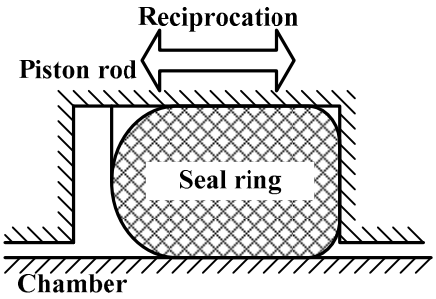

Figure 1. System of dynamic seal ring.

The seal ring is fixed in the slot of the piston rod and moves with the piston rod. Sometimes the seal ring is fixed in the slot in the chamber. However, it makes no difference in the calculation of the leakage amount for the dynamic seal ring. In this research, the chamber is assumed to be fixed. The relative motion is completed by a piston rod which reciprocates linearly in the axial direction. The framework of the leakage prediction calculation method is shown in Figure 2.

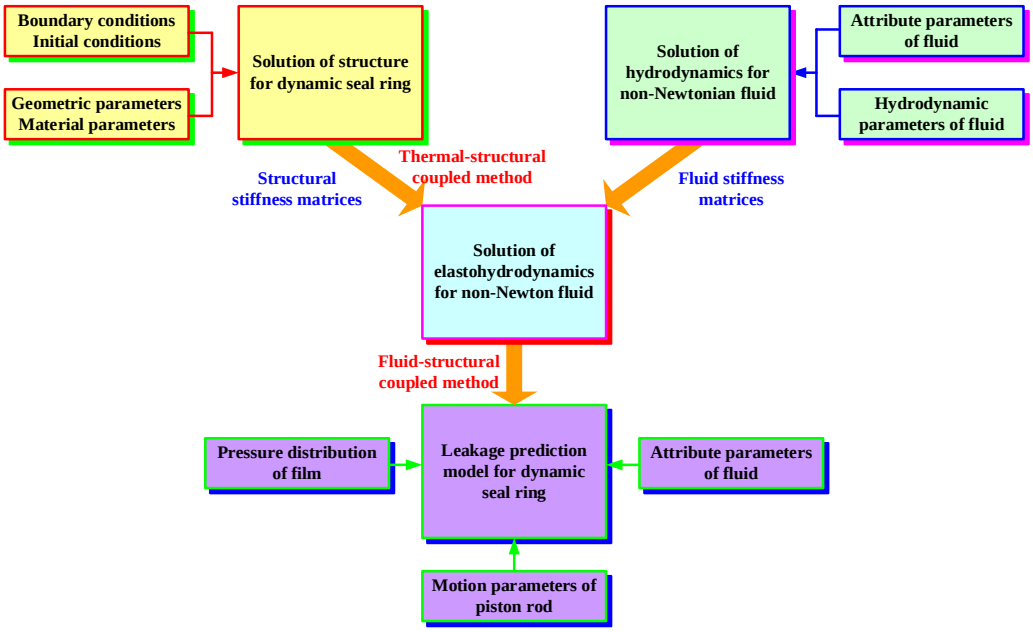

Figure 2. Framework of leakage prediction calculation method for dynamic seal ring in underground equipment.

Four modules are contained in the framework: the module of the solution for the structural domain of the dynamic seal ring, the module of the solution for the hydrodynamic domain of non-Newtonian fluid, the module of solution for the elasto-hydrodynamic (EHD) domain and the module of leakage prediction for dynamic seal ring. The final calculation

of the leakage prediction is completed by the module of leakage prediction. The output parameter of this module is the leakage amount of the dynamic seal ring, while the input parameters contain parameters of fluid attribute and motion of piston rod as well as pressure distribution of oil film in the sealing clearance.

The structural stiffness matrix, which is solved from the structural FE model, and the fluid stiffness matrix, which is solved from the hydrodynamic module of non-Newtonian fluid, are sent to the EHD module. Pressure distribution in the sealing clearance can be solved with the fluid–structural coupled method.

The FE model of the dynamic seal ring is built into the module of solution for the structural domain of the dynamic seal ring. Both boundary conditions and initial conditions according to the underground environment are adopted. The thermal–structural coupled method is applied to solve the FE model of the dynamic seal ring. Then, the structure stiffness matrix is output.

The module of solution for the hydrodynamic domain is in charge of solving the controlling equations of non-Newtonian fluid in the sealing clearance. Considering that the fluid in the underground environment is mostly non-Newtonian fluid, the hydrodynamic model for non-Newtonian fluid is adopted. The stiffness matrix of fluid in the sealing clearance can be output based on the FE method.

3. Leakage Prediction Model for Dynamic Seal Ring in Underground Equipment

In order to quantitatively determine the leakage amount of the dynamic seal ring when the piston rod reciprocates in a single cycle, the leakage amount will be analyzed separately when the piston rod is pushed out or pulled in. The distribution of oil film in the sealing clearance in both cases is shown in Figure 3.

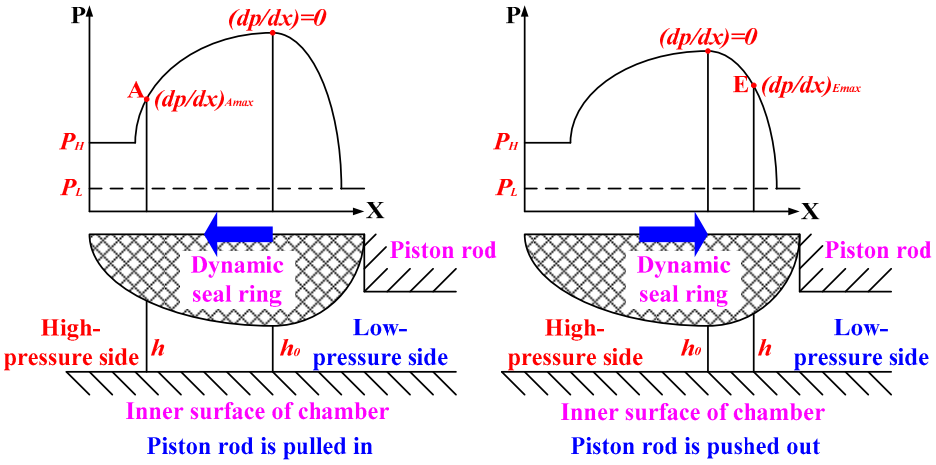

Figure 3. Distribution of oil film in the sealing clearance when piston rod is pushed out/pulled in.

The left side of the dynamic seal ring is assumed to be full of non-Newtonian fluid with higher pressure, while the other side is the lower-pressure side. Take the left picture in Figure 3, for example. When the thickness of oil film on a certain node A is h, the maximum of the pressure gradient reaches its maximum value $(dp/dx)_{A\max}$. The Reynolds equation for non-Newtonian fluid can be simplified as follows:

$$\frac{\partial}{\partial x}\left(\frac{h^3}{n\eta_e}\frac{\partial p}{\partial x}\right) = 6U\frac{\partial h}{\partial x} \tag{1}$$

where n is the power law exponent of non-Newtonian fluid, η_e is equivalent viscosity and U is the reciprocation velocity of the piston rod.

Integrate Equation (1):

$$h^3 \frac{\partial p}{\partial x} - 6n\eta_e U(h - h_0) = 0 \tag{2}$$

where h_0 is the thickness of the oil film when the pressure gradient is zero.

Taking a derivative with respect to the thickness of oil film h, a pressure gradient can be obtained as follows:

$$\frac{\partial p}{\partial x} = \frac{2n\eta_e U}{h^2} \tag{3}$$

According to Equations (2) and (3), it can be known that $h = (3/2)h_0$. Substituting this expression back into Equation (2), h_0 will be worked out as follows:

$$h_0 = \sqrt{\frac{8nU\eta_{eA}}{9\left(\frac{\partial p}{\partial x}\right)_{A\max}}} \tag{4}$$

The one-way leakage rate of the piston rod is as follows:

$$\dot{Q} = \frac{\pi d h_0 U}{2} \tag{5}$$

where d is the inner diameter of the chamber.

Substituting the expression of h_0 into Equation (5), the leakage rate for a dynamic seal ring in underground equipment can be given as follows:

$$\dot{Q} = \pi d U \sqrt{\frac{2nU\eta_{eA}}{9\left(\frac{\partial p}{\partial x}\right)_{A\max}}} \tag{6}$$

Similarly, when the piston rod is pushed out, the leakage rate of the dynamic seal ring can be expressed in the following form:

$$\dot{Q} = \pi d U \sqrt{\frac{2nU\eta_{eE}}{9\left(\frac{\partial p}{\partial x}\right)_{E\max}}} \tag{7}$$

The leakage amount in a single cycle can be expressed in the following form:

$$Q_s = \pi d L \left(\sqrt{\frac{2nU_i\eta_{eA}}{9\left(\frac{\partial p}{\partial x}\right)_{A\max}}} - \sqrt{\frac{2nU_o\eta_{eE}}{9\left(\frac{\partial p}{\partial x}\right)_{E\max}}} \right) \tag{8}$$

where L is the route of the piston rod.

The influence of high pressure and high temperature on leakage rate was not considered in Equation (8). Since both the pressure and the temperature underground are much higher than those on the ground, the effect of pressure and temperature on n and η_e should not be ignored.

There is an exponential relationship between equivalent viscosity and temperature, according to Gang [28]:

$$\eta_e = A_0 e^{\frac{B}{T}} \tag{9}$$

where A_0 and B are constants.

The relationship between equivalent viscosity and pressure is reflected through the effect of pressure on density, according to [29]. This effect can be expressed as follows:

$$\rho = \rho_0 \left(1 + \frac{C_1 P}{1 + C_2 P}\right) \tag{10}$$

where ρ_0 is the density of fluid at room temperature. P represents the pressure. C_1 and C_2 are constants, while $C_1 = 0.6 \times 10^{-9}$ Pa^{-1} and $C_2 = 1.7 \times 10^{-9}$ Pa^{-1}.

It needs to be explained that the density of fluid will also be affected by temperature. However, the density applied in this section is only used to build a connection between pressure and equivalent viscosity. The effect of temperature is already reflected in Equation (9).

With Equations (9) and (10), the relationship among equivalent viscosity, temperature and pressure can be expressed as follows:

$$\eta_e = A_1\left(1 + \frac{C_1 P}{1 + C_2 P}\right)e^{\frac{B}{T}} \tag{11}$$

There is also an exponential relationship between power law exponent and temperature, according to Li Y [30]:

$$n = rT^s \tag{12}$$

where r and s are constants.

So, the leakage prediction model of dynamic seal ring in underground equipment can be expressed as follows:

$$Q_s = \pi d L\left\{\sqrt{\frac{2AU_i T^s e^{\frac{B}{T}}\left(1 + \frac{C_1 P_A}{1+C_2 P_A}\right)}{9\left(\frac{\partial p}{\partial x}\right)_{A\max}}} - \sqrt{\frac{2AU_o T^s e^{\frac{B}{T}}\left(1 + \frac{C_1 P_E}{1+C_2 P_E}\right)}{9\left(\frac{\partial p}{\partial x}\right)_{E\max}}}\right\} \tag{13}$$

where A and B are constants.

4. Solution of the Structural FE Model for Dynamic Seal Ring

The modeling process is accomplished using the FE software ANSYS. Since the material of the chamber and piston rod is steel, which is much harder than rubber, the deformation of the chamber and piston rod can be neglected. Their profiles are treated as rigid constraints. Considering that rubber possesses the hyperelastic characteristic, the Mooney–Rivlin model is adopted.

The modeling process is comprised of two steps, as shown in Figure 4. In the first step, degrees of freedom in the x and z directions of the chamber profile are eliminated. Meanwhile, a displacement Δ in the z direction is set on the profile of the piston rod to generate an initial compression rate for the seal ring. The environmental temperature T is set as the initial condition. In the second step, fluid pressure P_f is set at nodes on the left side of the deformed seal ring. It is assumed that the left side beside the seal ring is the higher-pressure side, while the other side is the air side.

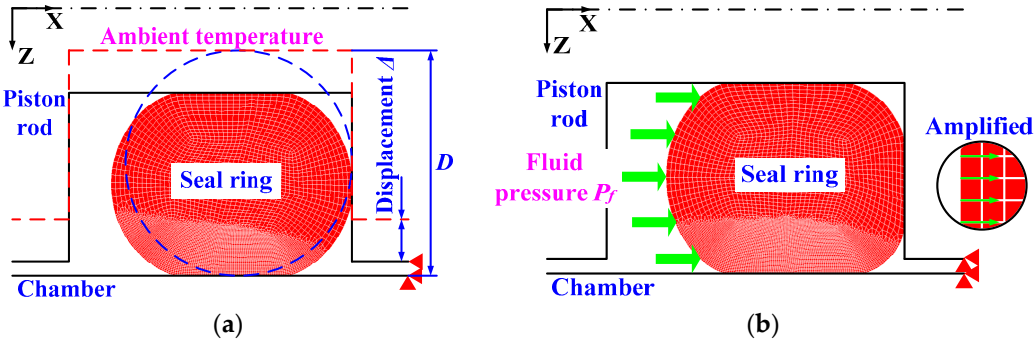

Figure 4. FE model of dynamic seal ring. (**a**) First step; (**b**) second step.

5. Interface Element of Non-Newtonian Fluid

By integrating Equation (2), hydrodynamic pressure in the oil film can be written as follows:

$$\begin{aligned} p^h(x) &= p_a + \int_{\xi=x_a}^{\xi=x} \frac{\partial p^h}{\partial \xi} d\xi \\ &= p_a + \int_{\xi=x_a}^{\xi=x} \frac{6n\eta_e U(h-h_0)}{h^3} d\xi \end{aligned} \tag{14}$$

where p_a and p_b are, respectively, pressure at the higher-pressure side and the air side with the assumption that $p_a < p_b$.

So, boundary conditions can be expressed as follows:

$$p^h(x_a) = p_a,\ p^h(x_b) = p_b \tag{15}$$

The viscous shear stress of the oil film can be expressed in the following form [31]:

$$\tau^h(x) = \frac{\eta_e U}{h} - \frac{h}{2}\left(\frac{\partial p^h}{\partial x}\right) \tag{16}$$

The clearance between the seal ring and the chamber is also the district where the oil film distributes, as shown in Figure 5. Therefore, the nodes on the edge of the seal ring in this district are affected by hydrodynamic pressure.

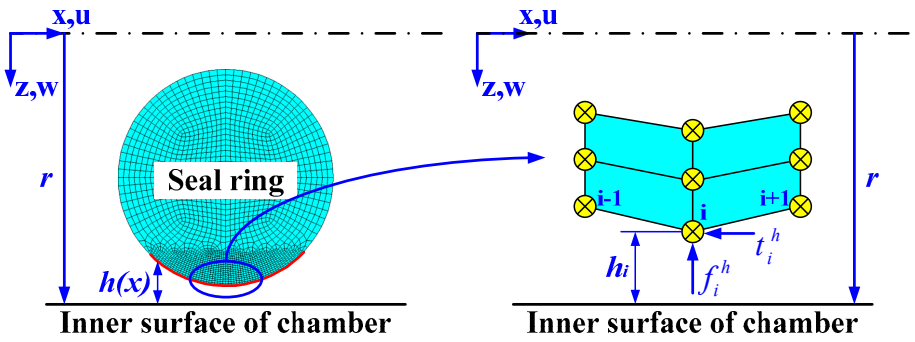

Figure 5. Interface element of non-Newtonian fluid.

In most cases, hydrodynamic pressure is solved with the Eular integral method:

$$\Delta x_i = (x_{i-1} + u_{i-1}) - (x_i + u_i) \tag{17}$$

where x_k is the coordinate of the interface nodes in the x direction. u_k is the displacement of the interface nodes in the x direction.

The recursive form of hydrodynamic pressure can be expressed as follows:

$$p_i^h = p_{i-1}^h + \left(\frac{\partial p^h}{\partial x}\right)_i \Delta x_i \tag{18}$$

The pressure gradient can be derived from Equation (2) as follows:

$$\left(\frac{\partial p^h}{\partial x}\right)_i = \frac{6n\eta_e U(h_i - h_0)}{h_i^3} \tag{19}$$

Finally, Equation (14) can be expressed in the form of numerical integration:

$$p_i^h = p_a + \sum_{k=2}^{i} \frac{6n\eta_e U(h_k - h_0)}{h_k^3} \Delta x_k \tag{20}$$

The thickness of the oil film at each node can be expressed in the following form:

$$h_i = r - (z_i + w_i) \tag{21}$$

where z_i is the coordinate of the i-th node in the z direction. w_i is the displacement of the i-th node in the z direction. r is the inner radius of the chamber.

The hydrodynamic pressure needs to be converted to nodal force set on the FE model:

$$f_i^h = p_i^h \cdot A_i \tag{22}$$

where A_i is the contacting area of the node. It can be expressed as follows:

$$A_i = \begin{cases} 0.5[(x_{i-1} + u_{i-1}) - (x_{i+1} + u_{i+1})], \ i = 2 \cdots m-1 \\ 0.5[(x_i + u_i) - (x_{i+1} + u_{i+1})], \quad i = 1 \\ 0.5[(x_{i-1} + u_{i-1}) - (x_i + u_i)], \quad i = m \end{cases} \tag{23}$$

Similarly, the shear force can be obtained through Equation (16):

$$t_i^h = \tau_i^h \cdot A_i \tag{24}$$

It should be noted that h_0 is the constant which needs to be solved by iteration. Residual error R is usually brought in to work out h_0 with the Newton–Raphson method:

$$R = p_a - p_b + \sum_{k=2}^{m} \frac{6n\eta_e U(h_k - h_0)}{h_k^3} \Delta x_k = 0 \tag{25}$$

6. Solution for EHD Domain of Non-Newtonian Fluid

6.1. Solution for FE Model

According to the virtual work principle, nonlinear equations can be obtained by discretizing the solution domain of the seal ring:

$$\overline{f}_i(\overline{u}_j) = 0 \tag{26}$$

where $\overline{f}_i$ is the vector of the overall residual forces. $\overline{u}_j$ is the vector of the overall nodal displacement.

It is defined that the symbol '¯' represents a global variable, while the symbol '~' represents an elemental variable. In the k-th iteration, the correction of the displacement vector of overall nodes can be expressed as follows:

$$\Delta \overline{u}_j^{k+1} = -[\overline{K}_{ij}^k]^{-1} \overline{f}_i \tag{27}$$

where $\overline{K}_{ij}^k$ is the stiffness matrix of the whole domain. So, the vector of the nodal displacement can be expressed as follows:

$$\overline{u}_j^{k+1} = \overline{u}_j^k + \Delta \overline{u}_j^{k+1} \tag{28}$$

The global stiffness matrix $\overline{K}_{ij}^k$ can be obtained by summing the stiffness matrix of all the elements in the domain of the seal ring. Therefore, the global stiffness matrix can be expressed in the following form:

$$\overline{K}_{ij}^k = \sum_{e=1}^{n^{el}} \widetilde{K}_{ij}^k \tag{29}$$

$$\widetilde{K}_{ij}^k = \frac{D\widetilde{f}_i^k}{D\widetilde{u}_j^k} \tag{30}$$

6.2. Stiffness Matrix of Non-Newtonian Fluid Interface Element

The loading vector of the interface element node can be obtained based on Equations (22), (24) and (25):

$$\widetilde{f}_i^h = \widetilde{f}_i^h\left(\widetilde{u}_j, h_0\right) = \left\{f_1^h, t_1^h, \cdots, f_m^h, t_m^h, R, 0\right\}^T \tag{31}$$

The stiffness matrix $\widetilde{K}_{ij}^h$ of the interface element can be obtained in the following expression:

$$\widetilde{K}_{ij}^h = \frac{D\widetilde{f}_i^h}{D\widetilde{u}_j^h} \tag{32}$$

$$\widetilde{u}_j^h = \{u_1, w_1, \cdots, u_m, w_m, h_0, 0\}^T \tag{33}$$

The derivation of hydrodynamic nodal force f_i^h at node I, with respect to radial displacement w_j at node j, can be written as follows:

$$\frac{Df_i^h}{Dw_j} = 6n\eta_e U A_i \Delta x_j \left(3h_0 h_j^{-4} - 2h_j^{-3}\right) \tag{34}$$

The derivation of nodal force with respect to axial displacement u_j at node j can be obtained in the same way:

$$\frac{Df_i^h}{Du_j} = \frac{\partial A_i}{\partial u_j} p_i^h + \sum_{k=2}^{i} \frac{6n\eta_e U(h_k - h_0)}{h_k^3} \frac{\partial \Delta x_k}{\partial u_j} \tag{35}$$

The derivation of nodal force with respect to integration constant h_0 can also be obtained as follows:

$$\frac{Df_i^h}{Dh_0} = 6n\eta_e U A_i \sum_{k=2}^{i} \left(-\frac{\Delta x_k}{h_k^3}\right) \tag{36}$$

The derivation of the shear force of the interface node can also be obtained in the same way as Equations (34)–(36):

$$\frac{Dt_i^h}{Dw_j} = A_i \left[-\frac{\eta_e U}{h_i^2} + \frac{1}{2}\left(\frac{\partial p^h}{\partial x}\right)_i + 3n\eta_e U h_i \left(3h_0 h_j^{-4} - 2h_j^{-3}\right)\right] \tag{37}$$

$$\frac{Dt_i^h}{Du_j} = \tau_i^h \frac{\partial A_i}{\partial u_j} \tag{38}$$

$$\frac{Dt_i^h}{Dh_0} = 3n\eta_e U A_i \left(-\frac{1}{h_i^2}\right) \tag{39}$$

At last, the stiffness matrix of the hydrodynamic interfacial element can be obtained by using residual error:

$$\frac{DR}{Dw_j} = 6n\eta_e U \Delta x_j \left(3h_0 h_j^{-4} - 2h_j^{-3}\right) \tag{40}$$

$$\frac{DR}{Du_j} = 6n\eta_e U \sum_{k=2}^{n} \frac{(h_k - h_0)}{h_k^3} \frac{\partial \Delta x_k}{\partial u_j} \tag{41}$$

$$\frac{DR}{Dh_0} = -6n\eta_e U \sum_{k=2}^{n} \frac{\Delta x_k}{h_k^3} \tag{42}$$

7. Development of Leakage Prediction Calculation Method for Dynamic Seal Ring in Underground Equipment

The development of the leakage prediction calculation method for dynamic seal rings in underground equipment is shown in Figure 6. In the beginning, the FE model of the seal ring is built and solved with the thermal–structural coupled method. The coordinates of the nodes in the domain of the seal ring as well as the structural stiffness matrix can be obtained. Then, parameters of fluid attribution, the velocity of the piston rod and an initial guess of h_0 are input to solve the Reynolds equation of non-Newtonian fluid to obtain the loading vector $\widetilde{f}_{ij}^{h}$ and stiffness matrix $\widetilde{K}_{ij}^{h}$ of the interface element. The stiffness matrix of the whole domain is obtained by summing the stiffness matrix of each interface element. Meanwhile, the global residual vector is obtained by integrating the loading vector in the fluid domain. Equation sets are solved using the Newton–Raphson method. If the solution converges, enter the next time step and recalculate the process above. Otherwise, return to the FE model and change the position of nodes as well as the initial guess of h_0. Repeat the process until the solution converges. When the calculating time is reached, the leakage amount of the dynamic seal ring is worked out according to the leakage prediction model.

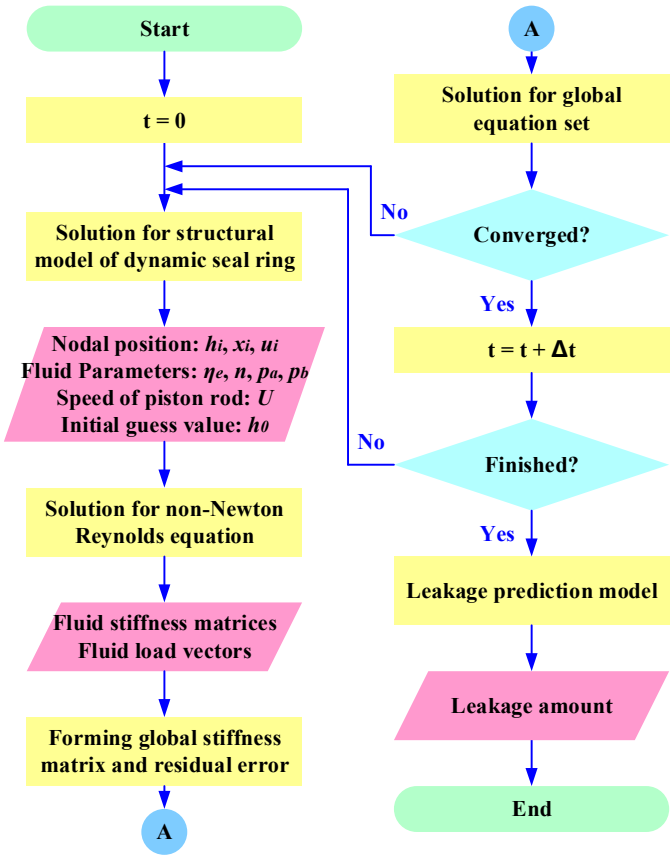

Figure 6. Development of leakage prediction calculation method for dynamic seal ring in underground equipment.

8. Test for Verification and Analysis of Results

8.1. Test

8.1.1. Test for Verification

To validate the proposed method, a test to measure the leakage amount under high temperature and high pressure is designed. The test system with high temperature and high pressure for seal rings is shown in Figure 7. Five modules are contained in the system: the linear motion driving module, heating module, pressure module, measurement module and controlling module.

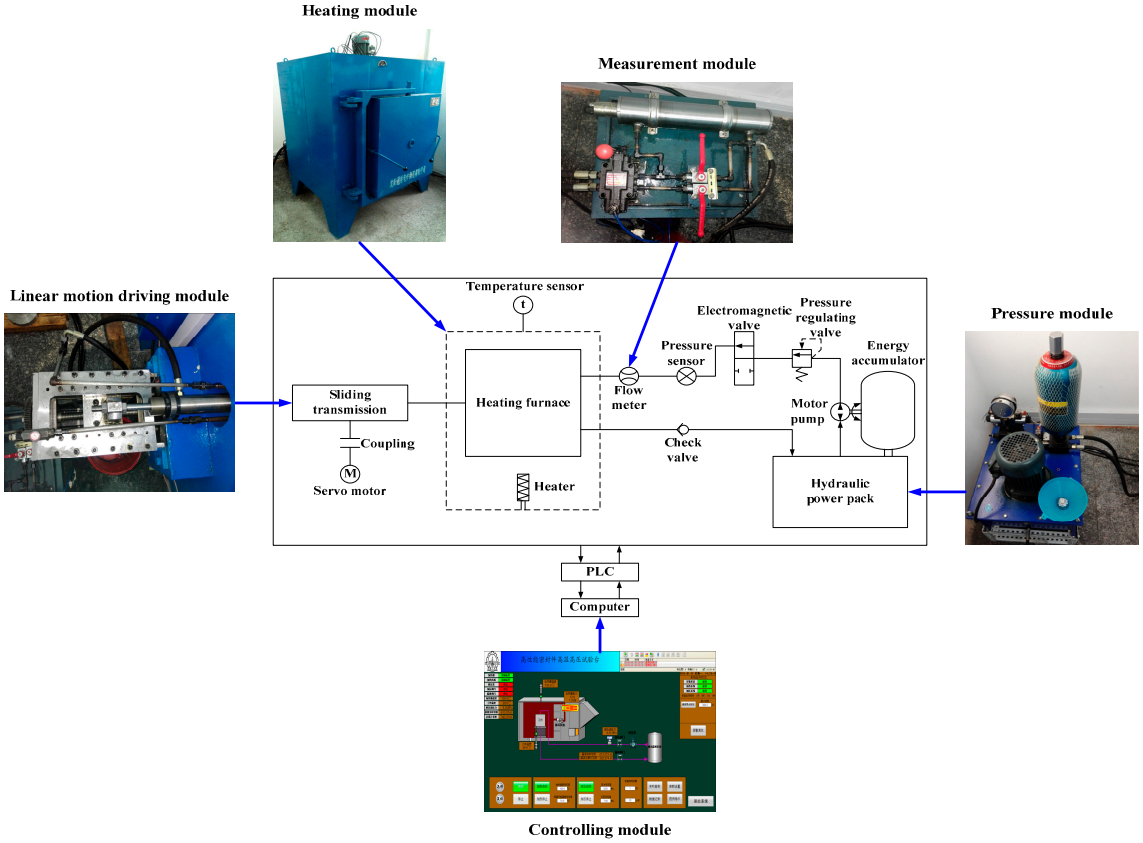

Figure 7. Test system with high temperature and high pressure for seal rings.

The designed test system is used to measure the leakage amount of seal rings under high temperatures and high pressure. Tested seal rings can be static seal rings as well as dynamic seal rings. The linear motion driving module is started to supply reciprocating motion when dynamic seal rings are tested. The heating module is applied to heat the fixture to a specified temperature. The pressure module is used to pump hydraulic oil with specified pressure into the fixture. The leakage amount of the seal rings is measured through the measurement module. The controlling module is in charge of controlling the four modules introduced above and recording the leakage amount every minute.

The fixture used in the test is shown in Figure 8. The main body of the fixture is a cylindrical chamber that has four holes on its external surface: one is for oil supply, one is for exhausting air, and the other two are for oil outflow. The inner diameter of the cylindrical chamber is 140 mm, while the external diameter is 195 mm.

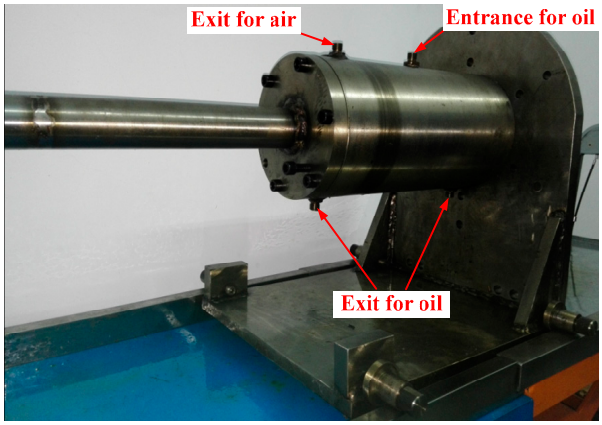

Figure 8. Fixture for dynamic seal ring.

The piston rod is shown in Figure 9a. Two seal rings are installed at each end of the piston rod, respectively. The diameter of the mounting groove for the seal ring is 135 mm, and the width of the mounting groove is 4.2 mm. Two kinds of dynamic seal rings used in the test are shown in Figure 9b. One is an O-ring made of nitrile rubber, and the other is an O-ring made of fluororubber. The sectional diameter of the seal ring is 2.65 mm, and the inner diameter is 134 mm.

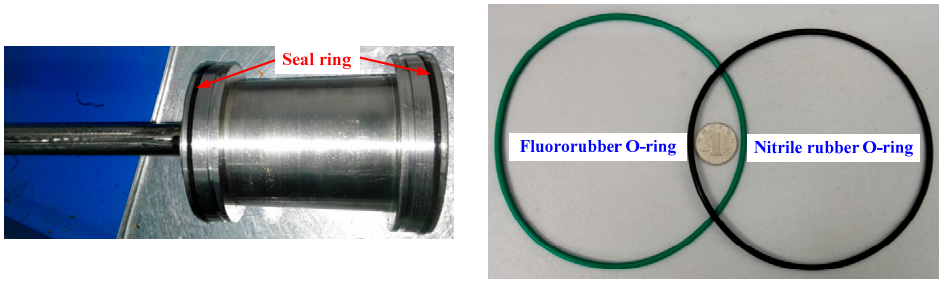

(**a**) (**b**)

Figure 9. Piston rod and tested dynamic seal rings. (**a**) Piston rod; (**b**) tested dynamic seal rings.

The fixture is laid in the heating furnace, as shown in Figure 10. The thermocouple is used to measure the temperature of the fixture. The piston rod is connected with the linear motion driving module through the hole in the wall of the heating furnace. The cylindrical chamber of the fixture is fixed to the external surface of the heating furnace. The piston rod will move reciprocally under the driving of the servo motor in the linear motion driving module.

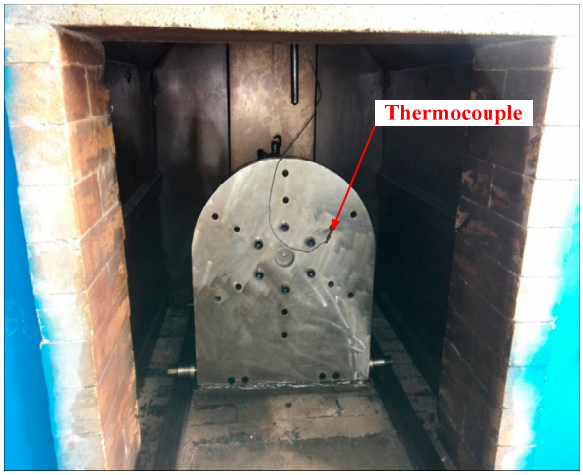

Figure 10. Fixture is laid in heating furnace.

8.1.2. Determination of Non-Newtonian Fluid Parameters

Determination of non-Newtonian fluid parameters can be fulfilled with the experimental method. The viscometer will be used. It is fixed in the heating furnace, as shown in Figure 11. The test is carried on under a specified temperature.

The equivalent viscosity of the non-Newtonian fluid can be expressed as follows:

$$\eta_e = \frac{0.31252n\rho}{3n+1}\left[\frac{t_{f43}(3n-1)}{n\left(h_4^{3-\frac{1}{n}} - h_3^{3-\frac{1}{n}}\right)}\right]^n v_{43}^{n-1} \tag{43}$$

where v_{43} is the average speed as the liquid level drops from h_4 to h_3.

The power law exponent can be expressed as follows:

$$n = \left[3 - \sqrt{\frac{\ln \frac{t_{f43}}{t_{f32}} \times \ln \frac{t_{f32}}{t_{f21}}}{\left(\ln \frac{h_4}{h_3}\right)^2}}\right]^{-1} \tag{44}$$

Considering that the density of the fluid is affected by temperature, the following expression is applied:

$$\rho = \rho_0[1 - C_3(T - T_0)] \tag{45}$$

where ρ_0 is the density of non-Newtonian fluid at 293 K, and the fluid selected is Shell TELLUSS2M46 hydraulic oil with ρ_0 = 0.89 g/cm^3. T is ambient temperature. T_0 is the reference temperature, while T_0 = 293 K. C_3 is a constant while C_3 = 0.00065 K^{-1}.

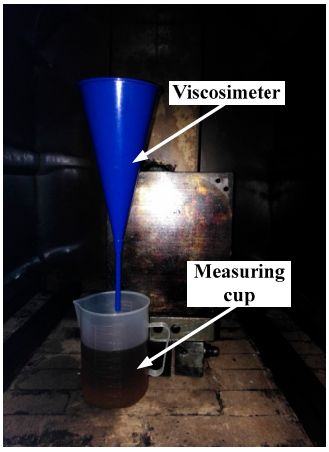

Figure 11. Viscometer fixed in heating furnace.

In this section, the relationship among equivalent viscosity, power law exponent of non-Newtonian fluid, and temperature will be illustrated. The outflow times of tested hydraulic oil at 353 K and 393 K are listed in Tables 1 and 2. To avoid the contingency of measuring time, four groups of outflowing time are measured. Additionally, the average values are adopted.

Table 1. Outflow time of tested hydraulic oil at 353 K.

	h_4~h_3			h_3~h_2			h_2~h_1		
	t_s	t_{fa}	t_f	t_s	t_{fa}	t_f	t_s	t_{fa}	t_f
1	12.0 s	6.0 s	6.0 s	9.1 s	4.2 s	4.9 s	6.2 s	3.0 s	3.2 s
2	11.6 s	6.0 s	5.6 s	8.8 s	4.2 s	4.6 s	6.7 s	3.0 s	3.7 s
3	12.2 s	6.0 s	6.2 s	8.7 s	4.2 s	4.5 s	6.3 s	3.0 s	3.3 s
4	11.8 s	6.0 s	5.8 s	8.6 s	4.2 s	4.4 s	6.8 s	3.0 s	3.8 s
Average	11.9 s	6.0 s	5.9 s	8.8 s	4.2 s	4.6 s	6.5 s	3.0 s	3.5 s

Table 2. Outflow time of tested hydraulic oil at 393 K.

	h_4~h_3			h_3~h_2			h_2~h_1		
	t_s	t_{fa}	t_f	t_s	t_{fa}	t_f	t_s	t_{fa}	t_f
1	10.7 s	6.0 s	4.7 s	7.8 s	4.2 s	3.6 s	5.9 s	3.0 s	2.7 s
2	10.8 s	6.0 s	4.8 s	8.1 s	4.2 s	3.9 s	6.0 s	3.0 s	3.0 s
3	10.7 s	6.0 s	4.7 s	8.0 s	4.2 s	3.8 s	5.6 s	3.0 s	2.6 s
4	11.0 s	6.0 s	5.0 s	7.7 s	4.2 s	3.5 s	5.9 s	3.0 s	2.9 s
Average	10.8 s	6.0 s	4.8 s	7.9 s	4.2 s	3.7 s	5..8 s	3.0 s	2.8 s

In addition, outflow time among 353 K and 393 K is also measured. The relationship between equivalent viscosity and temperature is obtained in Figure 12. An expression is worked out by fitting the discrete points as follows:

$$\ln(\eta_e) = \frac{2297.643}{T} - 10.849 \tag{46}$$

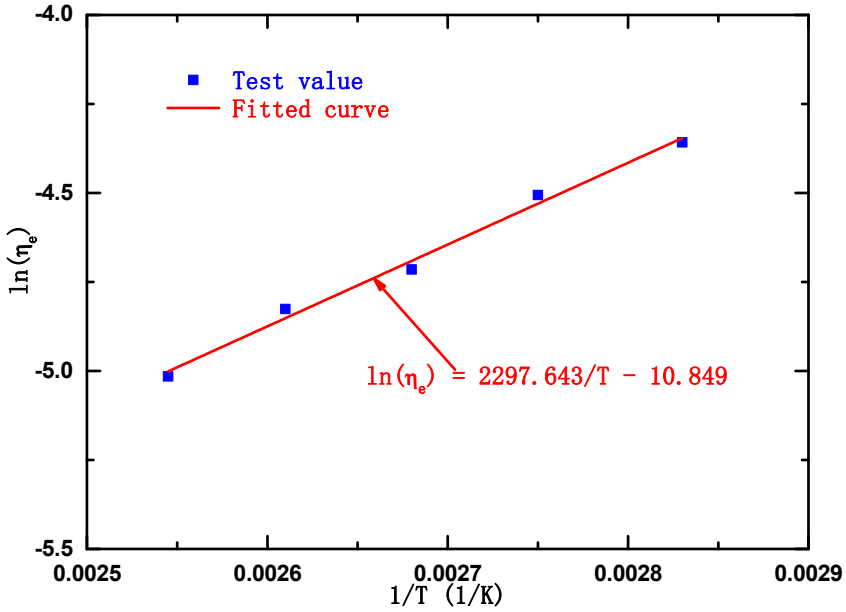

Figure 12. Relationship between equivalent viscosity and temperature.

Equation (11) can be modified as follows:

$$\ln(\eta_e) = \frac{B}{T} + \ln A + \ln\left(1 + \frac{C_1 P}{1 + C_2 P}\right) \tag{47}$$

Since the test is operated under standard atmospheric pressure, the influence of pressure can be ignored. So, the last item in Equation (47) is taken as zero. Comparing Equation (46) with Equation (47), we have the following: $A = 1.9424 \times 10^{-5}$, $B = 2297.643$. The equivalent viscosity is as follows:

$$\eta_e = 1.9424 \times 10^{-5} e^{\frac{2297.643}{T}} \left(1 + \frac{0.6 \times 10^{-9} P}{1 + 1.7 \times 10^{-9} P}\right) \tag{48}$$

The relationship between power law exponent and temperature is obtained from Figure 13:

$$n = 0.4904 T^{0.1355} \tag{49}$$

The unit of temperature is °C in the above equation. In order to unify the unit, Equation (49) is modified as follows:

$$n = 0.4904 (T - 273)^{0.1355} \tag{50}$$

Substituting Equations (48) and (50) into Equation (13), we can obtain the leakage prediction model of the dynamic seal ring in underground equipment:

$$Q_s = 0.0137 dL \left\{ \sqrt{\frac{U_i (T-273)^{0.1355} e^{\frac{2297.643}{T}} \left(1 + \frac{0.6 \times 10^{-9} P_A}{1 + 1.7 \times 10^{-9} P_A}\right)}{9 \left(\frac{\partial p}{\partial x}\right)_{A\max}}} - \sqrt{\frac{U_o (T-273)^{0.1355} e^{\frac{2297.643}{T}} \left(1 + \frac{0.6 \times 10^{-9} P_E}{1 + 1.7 \times 10^{-9} P_E}\right)}{9 \left(\frac{\partial p}{\partial x}\right)_{E\max}}} \right\} \tag{51}$$

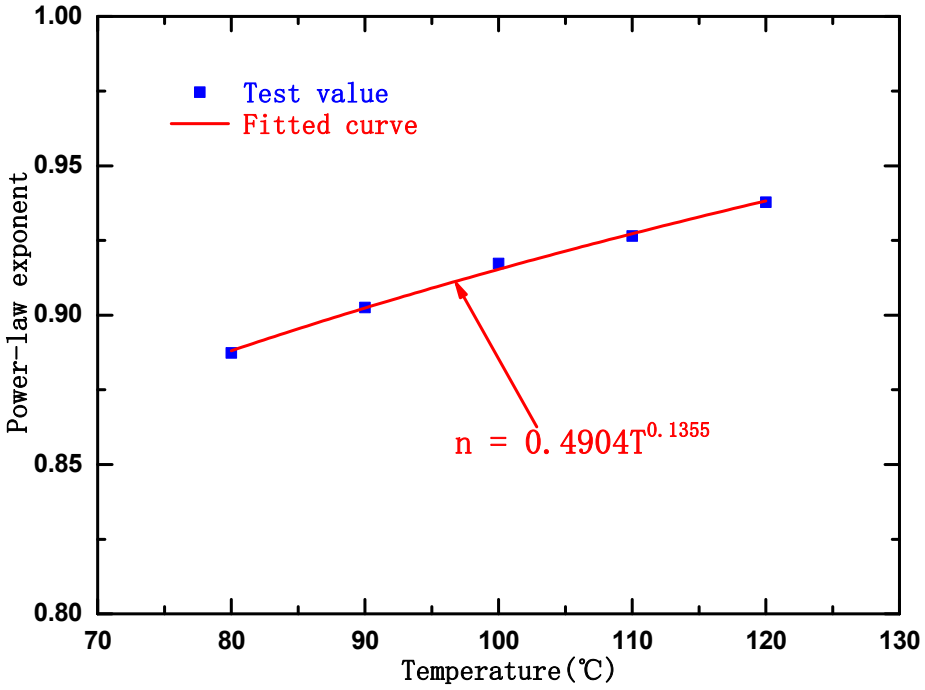

Figure 13. Relationship between power law exponent and temperature.

8.2. Hydrodynamic Characteristic of Oil Film in the Sealing Clearance

This section will take an O-ring made of nitrile rubber as an example to analyze the hydrodynamic characteristic of the oil film in the sealing clearance. The ambient temperature is 353 K, and the pressure is set as 12 MPa. The velocity of the piston rod is 10 cm/s. All the parameters needed in the calculation are listed in Table 3. The diameter of the section of the seal ring is 2.65 mm, and the compression of the seal ring is set as $\Delta = 2.65 - 2.4 - (140 - 139.8)/2 + 11.59 \times 10^{-6} \times [135/2 + (195 - 140)/2] = 0.1511$ mm.

Table 3. Parameters needed for the calculation.

Parameters	Value
Elasticity modulus of nitrile rubber, E	6.10 MPa
Poisson's ratio of nitrile rubber, ν	0.499
Parameter of Mooney-Rivlin model (353K), C_{10}	0.813 MPa
Parameter of Mooney-Rivlin model (353K), C_{01}	0.203 MPa
Coefficient of thermal expansion of nitrile rubber, α	1.6×10^{-4}/K
Ambient temperature, T	353 K

The distribution of fluid pressure in the sealing clearance is shown in Figure 14. It can be seen that when the piston rod is pulled in, the maximum pressure is greater than that when the piston rod is pushed out. The distribution of film thickness is shown in Figure 15. When the piston rod is pulled in, the film thickness is greater than that when the piston rod is pushed out. The reason for this is related to the distribution of fluid pressure. When the piston rod is pushed out, hydrodynamic pressure is smaller. The surface of the seal ring squeezes the fluid to reduce the deformation. A new equilibrium between hydrodynamic pressure and deformation stress is built. So, the clearance of the sealing region is reduced, and the film thickness is reduced as well.

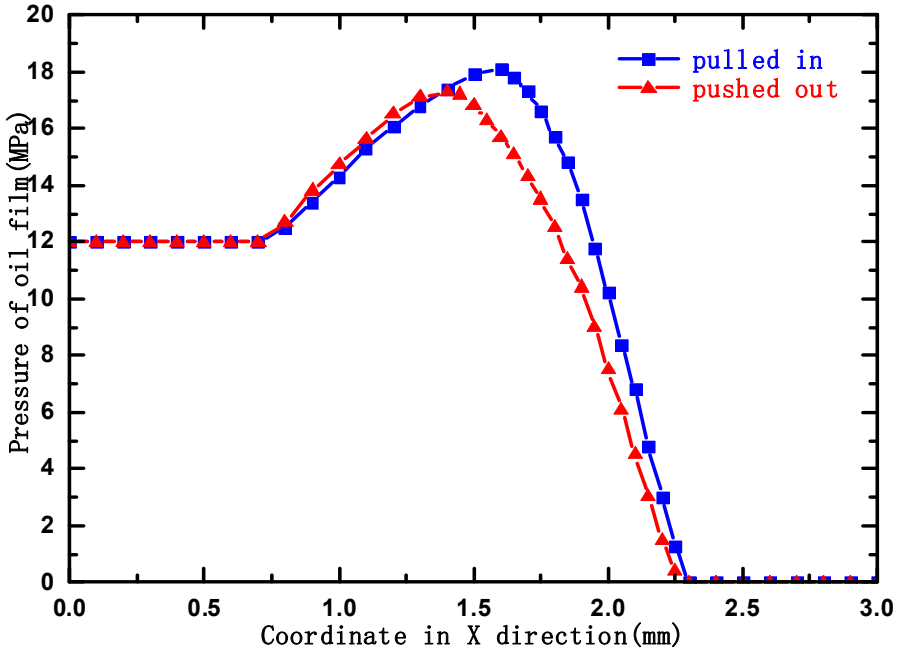

Figure 14. Distribution of fluid pressure when the piston rod is pulled in/pushed out.

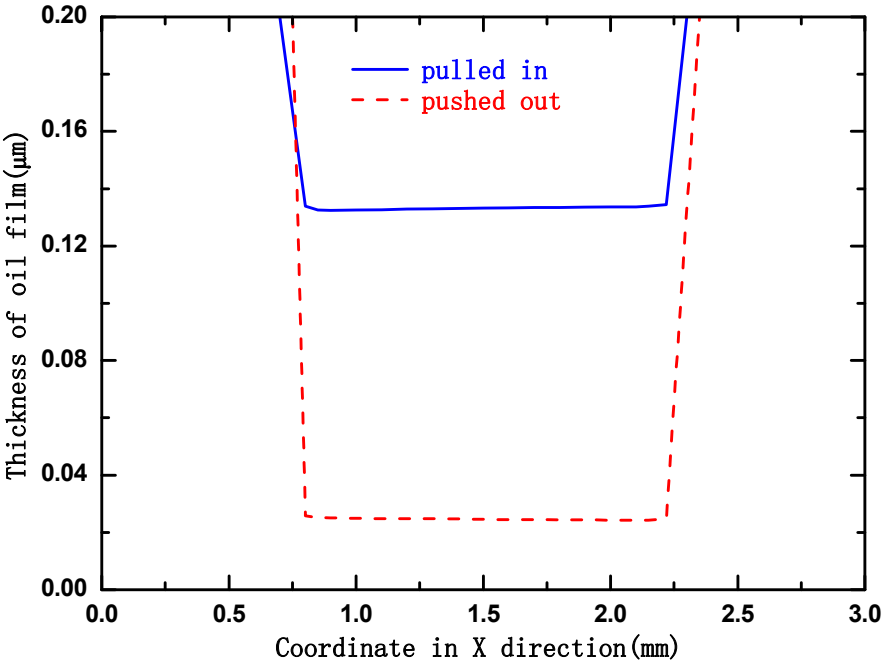

Figure 15. Distribution of film thickness when the piston rod is pulled in/pushed out.

8.3. Comparison and Analysis of the Results

According to the leakage prediction model, the parameters needed are listed as follows: The inner diameter of the chamber d = 14 cm, the one-way stroke of the piston rod is 20 cm, the velocity of the piston rod is 10 cm/s, the power law exponent of oil at the temperature 353 K is n = 0.888, the hydrodynamic pressure at node A when the piston rod is pulled in is P_A = 15.8 MPa and its highest pressure gradient $(\partial p/\partial x)_{A\max}$ = 61.1 MPa/cm, the hydrodynamic pressure at node E when the piston rod is pushed out is P_E = 9.6 MPa and its highest pressure gradient $(\partial p/\partial x)_{E\max}$ = 226.7 MPa/cm, the equivalent viscosity at node A at 353 K is η_A = 0.0132 Pa·s and equivalent viscosity at node E at 353 K is η_E = 0.0131 Pa·s.

By substituting all the parameters into the leakage prediction model, the leakage amount of a single cycle can be obtained:

$$\begin{aligned} Q_s &= \pi \times 14 \times 20 \times \sqrt{\frac{2\times 0.888\times 10}{9}}\left(\sqrt{\frac{0.0132}{61.1\times 10^6}} - \sqrt{\frac{0.0131}{226.7\times 10^6}}\right) \\ &= 8.77 \times 10^{-3}\text{mL} \end{aligned} \tag{52}$$

When the piston rod reciprocates for one cycle, the leakage amount is 8.77×10^{-3} mL. According to the fixture used in the test, two dynamic seal rings with the same specification are fixed at both ends of the piston rod, respectively. Therefore, the travel distance of the piston rod to move one way equals the distance of a single seal ring moving reciprocally. So, the leakage amount during the one-way motion of the piston rod equals the leakage amount during the reciprocation of one seal ring. The time for one-way travel is 2 s. Therefore, one seal ring can make 30 reciprocation travels in one minute. In every minute, the leakage amount is $8.77 \times 10^{-3} \times 30 = 0.263$ mL. So, in 30 min, the leakage amount will be $0.263 \times 30 = 7.89$ mL.

A comparison of the leakage amount between the predicted value and test value is shown in Figure 16. We can see that the predicted value is slightly bigger than the test value. That is because as the fluid leaks, the fluid pressure in the fixture is decreased gradually. The reduction in pressure difference leads to a smaller leakage. However, the prediction result is still able to reflect the trend of the leakage amount properly.

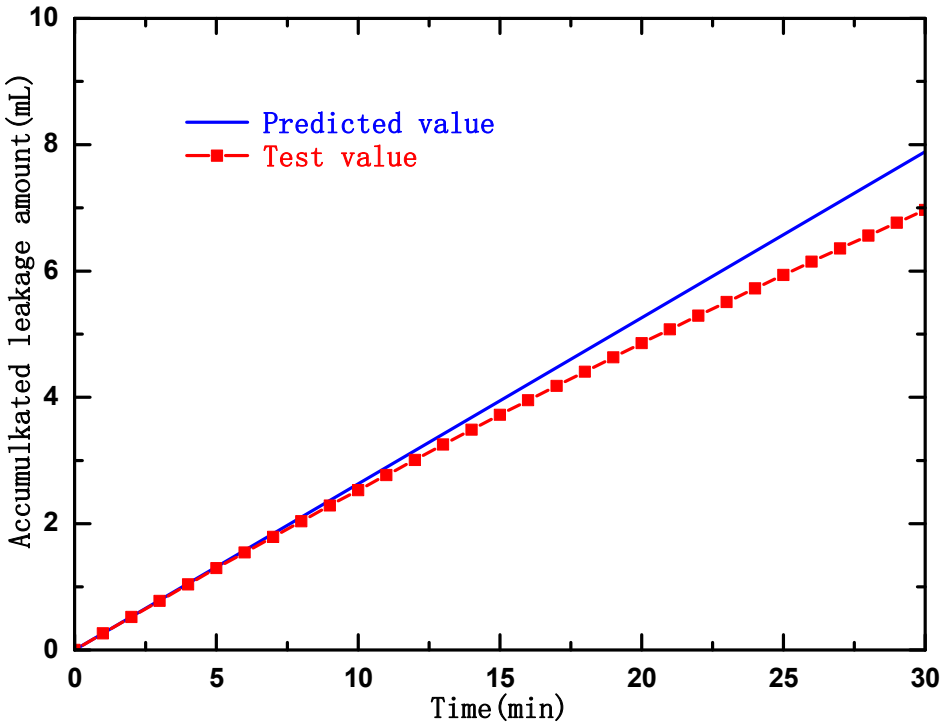

Figure 16. Comparison between predicted value and test value for nitrile rubber O-ring (353 K, 12 MPa and 10 cm/s).

In order to verify the proposed calculation method, comparisons between the predicted value and test value are also performed on the O-ring made of nitrile rubber under other environmental conditions. The leakage amount of the seal ring under the conditions (353 K, 16 MPa and 15 cm/s), (373 K, 12 MPa and 15 cm/s) and (373 K, 12 MPa and 10 cm/s) is, respectively, shown in Figures 17–19. We can see that the predicted results agree well with the test results.

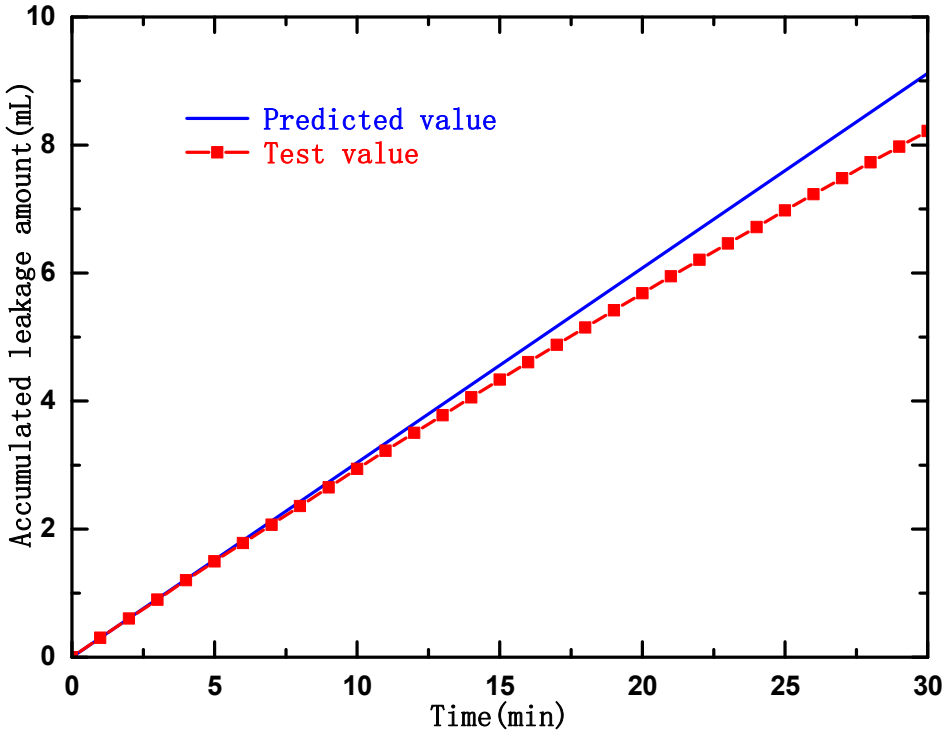

Figure 17. Comparison between predicted value and test value for nitrile rubber O-ring (353 K, 16 MPa and 15 cm/s).

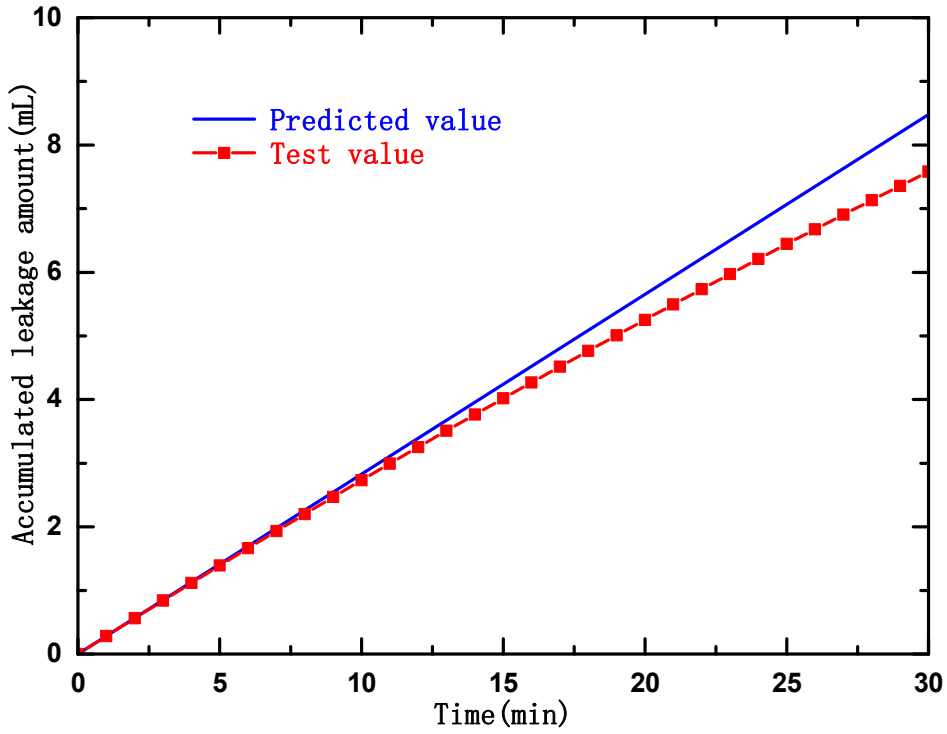

Figure 18. Comparison between predicted value and test value for nitrile rubber O-ring (373 K, 12 MPa and 15 cm/s).

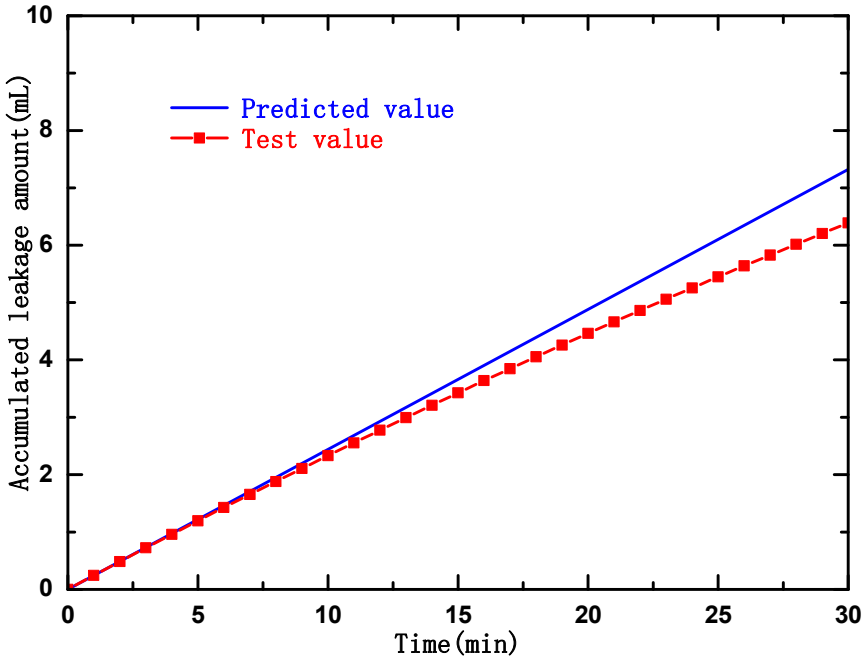

Figure 19. Comparison between predicted value and test value for nitrile rubber O-ring (373 K, 16 MPa and 10 cm/s).

Comparisons are also performed on the O-ring made of fluororubber, as shown in Figures 20–23. Compared with nitrile rubber, the leakage amount of O-ring made of fluororubber is slightly bigger in the same environmental conditions. The reason for this is that the elasticity modulus of fluororubber is bigger than that of nitrile rubber. The deformation of the O-ring made of fluororubber is smaller than that made of nitrile rubber when bearing the same pressure. So, the contact pressure of the O-ring made of fluororubber is smaller than that made of nitrile rubber. There is a slightly larger clearance for the O-ring made of fluororubber in the sealing region, which leads to a larger leakage amount.

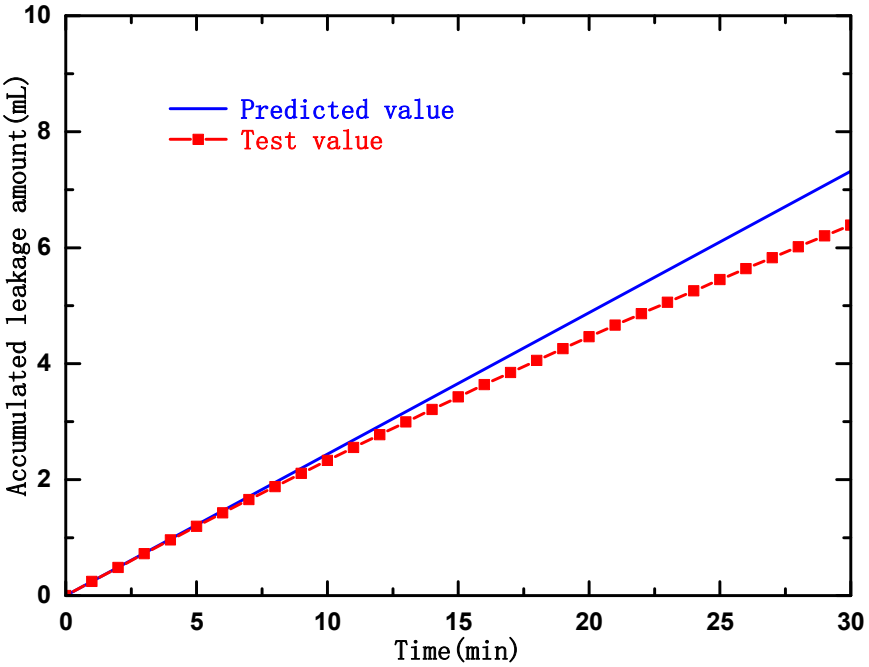

Figure 20. Comparison between predicted value and test value for fluororubber O-ring (353 K, 12 MPa and 10 cm/s).

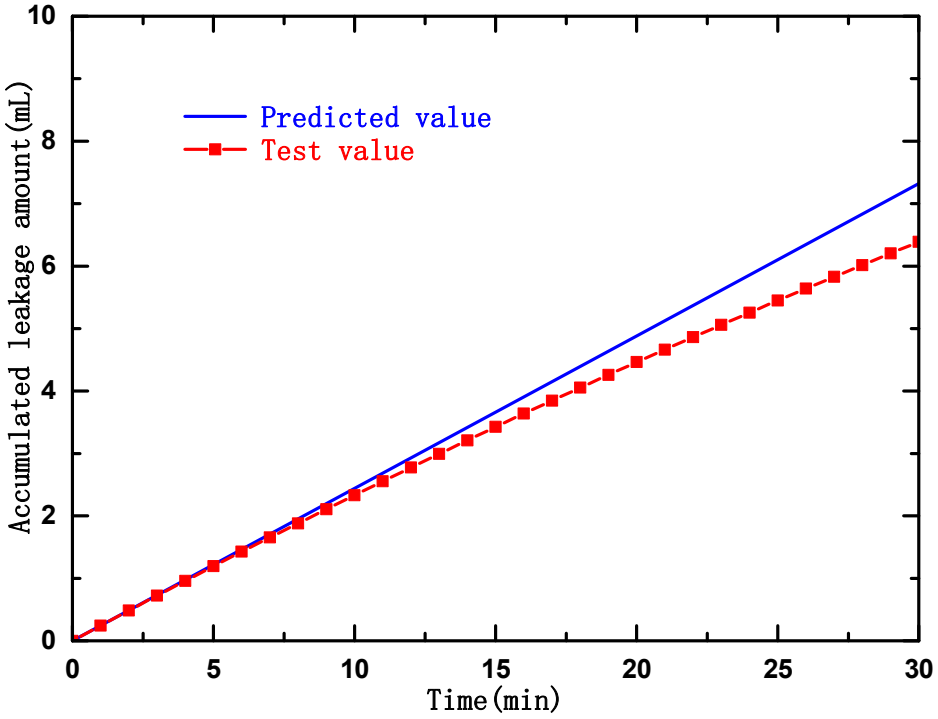

Figure 21. Comparison between predicted value and test value for fluororubber O-ring (353 K, 16 MPa and 15 cm/s).

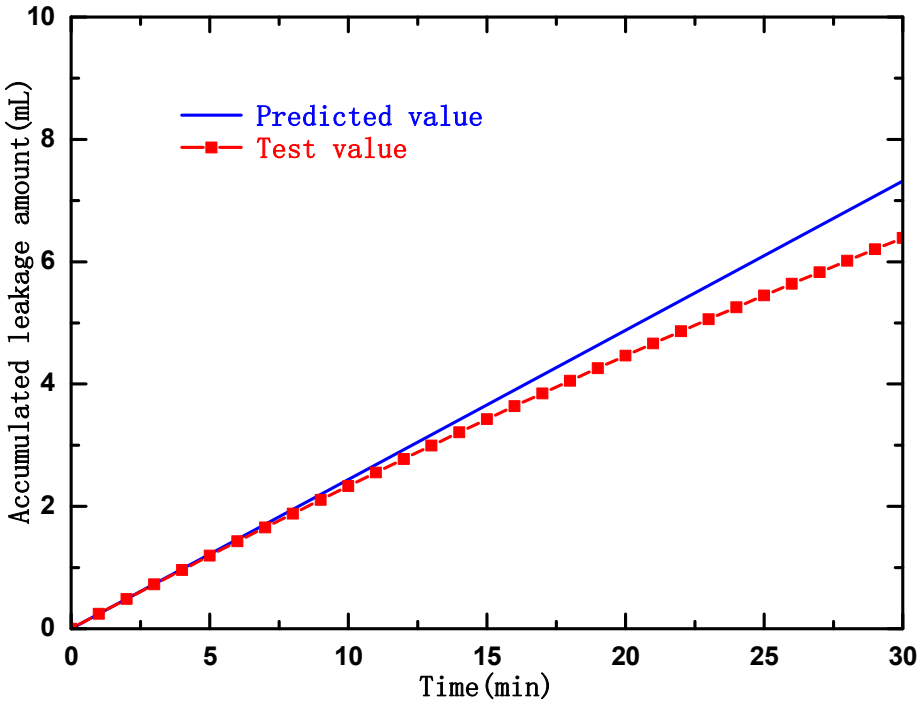

Figure 22. Comparison between predicted value and test value for fluororubber O-ring (373 K, 12 MPa and 15 cm/s).

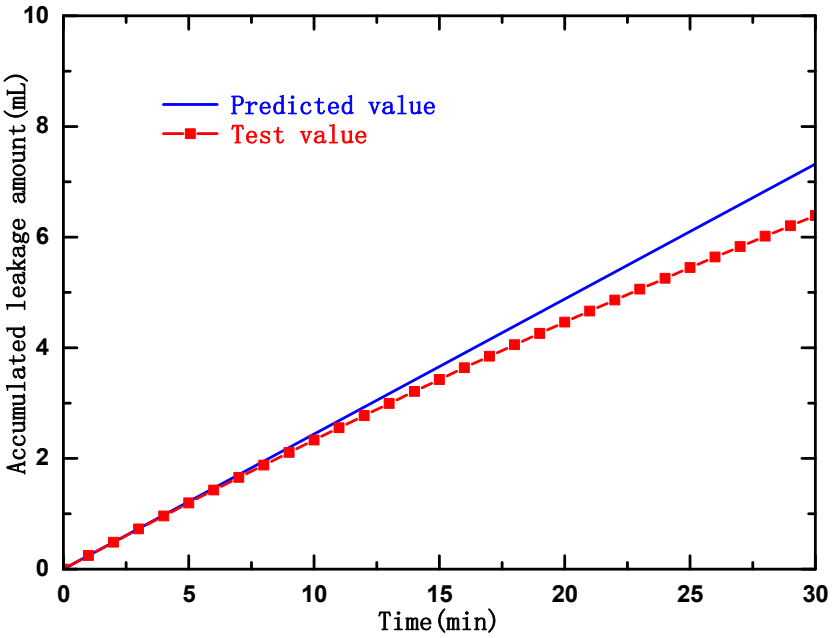

Figure 23. Comparison between predicted value and test value for fluororubber O-ring (373 K, 16 MPa and 10 cm/s).

9. Conclusions

The leakage prediction calculation method for dynamic seal rings in underground equipment is presented in this paper. The following work was accomplished:

(1) A Framework of the method was given;
(2) A leakage prediction model for dynamic seal rings in underground equipment was built. Non-Newtonian fluid interface elements were brought in;
(3) Development of the leakage prediction calculation method was given;
(4) A test was performed to validate the proposed method.

The results suggested that the film thickness of an O-ring made of nitrile rubber in pulling-in travel is thicker than that in pushing-out travel. The leakage of an O-ring made of fluororubber is larger than that of an O-ring made of nitrile rubber in the same environmental condition. The presented method is useful for predicting the sealing ability of dynamic seal rings in underground equipment.

In the underground environment, dynamic seal rings may be in a mixed lubrication state. The leakage prediction calculation method for dynamic seal rings in underground equipment based on mixture lubrication will be the future research direction for the authors.

Author Contributions: The main work was accomplished by X.X. and X.L., while the test was carried out by F.W. and C.X. All authors have read and agreed to the published version of the manuscript.

Funding: This work is supported by the Anhui University Natural Science Research Project (No. KJ2020A0359), the Fund of Introducing Talent People of Anhui Polytechnic University (No. 2020YQQ007, No. 2020YQ017) and Anhui Future Technology Research Institute Enterprise Cooperation Project (No. 2023qyhz19).

Data Availability Statement: Not applicable.

Conflicts of Interest: The authors declare no conflict of interest.

References

1. Saychenko, L.; Tananykhin, D.; Ashena, R. Prevention of scale in the downhole equipment and productive reservoir during the oil well operation. *J. Appl. Eng. Sci.* **2021**, *19*, 363–368. [CrossRef]
2. Xie, H.; Konietzky, H.; Zhou, H.W. Special issue "deep mining". *Rock Mech. Rock Eng.* **2019**, *52*, 1415–1416. [CrossRef]

3. Gao, M.; Xie, J.; Gao, Y.; Wang, W.; Li, C.; Yang, B.; Liu, J.; Xie, H. Mechanical behavior of coal under different mining rates: A case study from laboratory experiments to field testing. *Int. J. Min. Sci. Technol.* **2021**, *31*, 825–841. [CrossRef]
4. Xie, H.P.; Liu, T.; Gao, M.Z.; Chen, L.; Zhou, H.W.; Ju, Y.; Gao, F.; Peng, X.B.; Li, X.J.; Peng, R.D.; et al. Research on in-situ condition preserved coring and testing systems. *Pet. Sci.* **2021**, *18*, 1840–1859. [CrossRef]
5. Zaripova, L.M.; Gabdrakhimov, M.S. A mathematical model of the pulsator for cleaning paraffin deposits of pipe-lines and downhole equipment. *J. Phys. Conf. Ser.* **2019**, *1333*, 032095. [CrossRef]
6. Xie, H.P. Research framework and anticipated results of deep rock mechanics and mining theory. *Adv. Eng. Sci.* **2017**, *49*, 1–16.
7. Gao, M.Z.; Liu, J.J.; Lin, W.M.; Deng, G.; Peng, G.; Li, C.; He, Z. Study on in-situ stress evolution law of ultra-thick coal seam in advance mining. *Coal Sci. Technol.* **2020**, *48*, 8.
8. Gao, M.; Wang, M.; Xie, J.; Gao, Y.; Deng, G.D.; Yang, B.; Wang, F.; Hao, H.; Xie, H. In-situ disturbed mechanical behavior of deep coal rock. *J. China Coal Soc.* **2020**, *45*, 2691–2703.
9. Gao, M.; Xie, J.; Guo, J.; Lu, Y.; He, Z.; Li, C. Fractal evolution and connectivity characteristics of mining-induced crack networks in coal masses at different depths. *Geomech. Geophys. Geo-Energy Geo-Resour.* **2021**, *7*, 9. [CrossRef]
10. Xie, H.; Gao, F.; Ju, Y. Research and development of rock mechanics in deep ground engineering. *Chin. J. Rock Mech. Eng.* **2015**, *34*, 2161–2178.
11. Yin, Q.; Wu, J.; Zhu, C.; He, M.; Meng, Q.; Jing, H. Shear mechanical responses of sandstone exposed to high temperature under constant normal stiffness boundary conditions. *Geomech. Geophys. Geo-Energy Geo-Resour.* **2021**, *7*, 35. [CrossRef]
12. Yin, Q.; Wu, J.; Zhu, C.; Wang, Q.; Zhang, Q.; Jing, H.; Xie, J. The role of multiple heating and water cooling cycles on physical and mechanical responses of granite rocks. *Geomech. Geophys. Geo-Energy Geo-Resour.* **2021**, *7*, 69. [CrossRef]
13. Gao, M.Z.; Zhang, J.G.; Li, S.W.; Wang, M.; Wang, Y.W.; Cui, P.F. Calculating changes in fractal dimension of surface cracks to quantify how the dynamic loading rate affects rock failure in deep mining. *J. Cent. South Univ.* **2020**, *27*, 3013–3024. [CrossRef]
14. Feng, G.; Kang, Y.; Meng, T.; Hu, Y.Q.; Li, X.H. The influence of temperature on mode I fracture toughness and fracture characteristics of sandstone. *Rock Mech. Rock Eng.* **2017**, *50*, 2007–2019. [CrossRef]
15. He, Z.Q.; Chen, L.; Lu, T.; Xie, J. The optimization of pressure controller for deep earth drilling. *Therm. Sci.* **2019**, *23* (Suppl. S3), 877–885. [CrossRef]
16. Ahmed, S.; Patel, H.; Salehi, S. Numerical modeling and experimental study of elastomer seal assembly in downhole wellbore equipment: Effect of material and chemical swelling. *Polym. Test.* **2020**, *89*, 106608. [CrossRef]
17. Zhu, X.; Jing, Y. Analysis of Main Influence Factors for Slip Ring Combined Rotating Seals Based on 3D Contact. *China Mech. Eng.* **2017**, *28*, 1548.
18. Guo, Y.; Wu, L.; Xu, H.; Zeng, L.; Zhan, C. Analysis of dynamic sealing performance of Glyd ring and optimization of sealing parameters. *Lubric. Eng.* **2021**, *46*, 17–25.
19. Zhao, L.; Suo, S.F.; Shi, J.W. Design and research of high-pressure rotary combined seal test device. *Lubric. Eng.* **2020**, *45*, 12.
20. Salant, R.F.; Maser, N.; Yang, B. Numerical model of a reciprocating hydraulic rod seal. *Int. Jt. Tribol. Conf.* **2006**, *42592*, 577–583.
21. Nikas, G.K.; Sayles, R.S. Computational model of tandem rectangular elastomeric seals for reciprocating motion. *Tribol. Int.* **2006**, *39*, 622–634. [CrossRef]
22. Chen, B.; Yang, X.; Tu, Q. The sealing performance of cap-shape ring combined seal. *Lubric. Eng.* **2019**, *44*, 92–98.
23. Blasiak, S.; Laski, P.A.; Takosoglu, J.E. Parametric analysis of heat transfer in non-contacting face seals. *Int. J. Heat Mass Transf.* **2013**, *57*, 22–31. [CrossRef]
24. Mo, L.; Wang, J.; Guan, X.Q. Analysis of dynamic sealing characteristics of O-ring in petroleum machinery. *Chin. Petrol. Mach* **2014**, *42*, 103–107.
25. Sukumar, T.; Subramanian, M.; Subramaniyan, S.K.; Subramanian, N. *Design and Optimization of Lip Seal for Air Braking System*; SAE Technical Paper; SAE International: Warrendale, PA, USA, 2015.
26. Chen, H.L.; Liu, J.F.; Ren, K.T.; Li, T.; Fu, J.; Zou, Q.; Yin, Y.X. Optimization of upstream pumping mechanical seal based on response surface method. *J. Drain. Irrig. Mach. Eng.* **2016**, *34*, 232–237.
27. Ahmed, S.; Salehi, S.; Ezeakacha, C.; Teodoriu, C. Experimental investigation of elastomers in downhole seal elements: Implications for safety. *Polym. Test.* **2019**, *76*, 350–364. [CrossRef]
28. Gang, X.; Yong, L.; Jiu-Shun, C.; Li-Yu, D. Rheological property of Aqueous Partially Hydrolyzed Polyacrylamide Solution. *Chi-Nese J. Appl. Chem.* **2000**, *17*, 72–74.
29. Li, X.; Li, C.; Shu, A.; Xie, Y. Measuring rheological parameters of power law fluid by funnel viscometer. *Nat. Gas Ind.* **2003**, *23*, 47–50.
30. Li, Y.; Zhang, K.; Wang, Y.Z.; Wang, L.N. Apparent viscosity model of power law fluid flow in heavy oil wells. *Shiyou Kantan Yu Kaifa (Pet. Explor. Dev.)* **2007**, *34*, 616–621.
31. Schmidt, T.; André, M.; Poll, G. A transient 2D-finite-element approach for the simulation of mixed lubrication effects of recip-rocating hydraulic rod seals. *Tribol. Int.* **2010**, *43*, 1775–1785. [CrossRef]